Future Electronic Power Distribution Systems – A contemplative view –

Dushan Boroyevich, Igor Cvetković, Dong Dong, Rolando Burgos, Fei Wang, Fred Lee
Center for Power Electronics Systems (CPES)
The Bradley Department of Electrical and Computer Engineering
Virginia Tech, Blacksburg, VA 24061-0179, USA; Email: dushan@vt.edu

***Abstract*—Although it has long been argued that electronic power converters can help improve system controllability, reliability, size, and efficiency, their penetration in power systems is still quite low. The often-cited barriers of higher cost and lower reliability of the power converters are quite high if power electronics is used as direct, one-to-one, replacement for the existing electromechanical equipment. However, if the whole power distribution system were designed as a system of controllable converters, the overall system cost and reliability could actually improve, as is currently the case at low power levels within computer and telecom equipment.**

Starting from the example of a computer power system, the paper contemplates possible future ac and dc electronic power distribution system architectures, especially in the presence of renewable energy sources. The proposed nanogrid–microgrid–…–grid structure achieves hierarchical dynamic decoupling of generation, distribution, and consumption by using bidirectional converters as energy control centers. This is illustrated by the description and simulation of static and dynamic operation of a dc nanogrid in a hypothetical future sustainable home. Several ideas for modeling, analysis, and system-level design of such systems, including power flow control, protection, stability, and subsystem interactions, are presented.

***Index Terms*—electronic power converters, electric power distribution, power conversion systems, power converter modeling, system integration, nanogrid, microgrid, intergrid.**

I. Introduction

In traditional electrical power systems, the dynamics of generation (sources), distribution, and consumption (loads) are fully coupled. The system stability must then be passively assured by imposing overwhelmingly slow dynamics of the sources: electromechanically anchored constant frequency of the rotating synchronous generators in ac systems or electrochemically-anchored constant voltage of the batteries in dc systems. Availability of energy to the loads is only ensured through redundancy, over-design, and electromechanically (switchgear) controlled system reconfiguration and protection. These systems are considered to be inherently slow, inefficient, and unreliable [1].

In the past, power electronics converters have been mostly employed for local power conversion from an "infinite" source to meet dynamic energy demands of a specific load. Only recently, power converters are starting to be used *to decouple the dynamics between sources, distribution system, and loads*. For example, the growing need for a highly reliable supply of electrical energy for critical applications, such as hospitals, datacom centers, and semiconductor industry, has spawned the development of super-reliable local power distribution systems with the extended use of power electronics converters. These systems include multiple primary and secondary energy sources, several levels of energy storage and back-up, and numerous active loads, all interfaced through *electronic* power converters [2]-[4].

Similarly, there has been increased incorporation of power electronics converters in "more electric" cars, ships, and airplanes to replace thermo-mechanical, mechanical, hydraulic, and pneumatic primary and secondary power systems [5]-[8]. The goals have been to reduce the size, weight, and maintenance and operational costs of these power systems, while increasing efficiency, safety, reliability, and optimizing mission-specific objectives (payload, autonomy, survivability), as well as to enable the usage of alternative energy sources, e.g. fuel cells. In these applications, majority of energy sources are interfaced to the power system through power electronics converters because of their very different dynamic characteristics. Single or multiple power conversion stages are used to interconnect all subsystems that distribute energy to multitudes of different load converters ranging in power from few watts to hundreds of kilowatts.

Higher power applications also follow similar trends [9]-[11]. All of the emerging alternative and renewable energy sources are interfaced to the existing power systems through power electronics converters because of their very different dynamic characteristics. For example, in wind farms and distributed generation in general, power converters are used to interface the energy sources to the grid, and also to supplant the grid when it is absent or economical to do. The use of full ac-to-ac power conversion interface for wind generators has become a feasible option to replace doubly-fed induction generators with indirect interfacing [2], [12].

Based on these examples, it could be envisioned that in future *electronic power distribution systems* (EPDS), the dynamics of electric energy generation, distribution, and delivery will be fully dynamically decoupled by using separate *source converters*, *load converters*, and *power distribution converters*. As an illustration (and inspiration) of this approach, consider a notebook PC power management system depicted in Fig. 1. Instead of forcing all components inside a computer to use a single voltage supply – as was the case with 5 V logic in the past – most of the loads are now fed from a dedicated power supply with a voltage (e.g. 0.7, 1.8,

978-1-4244-7020-4/10/$26.00 ©2010 IEEE

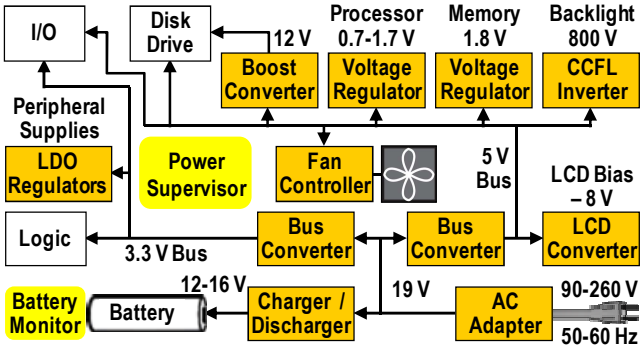

Fig. 1. A notebook power system.

3.3, -8, 800 V) and dynamic behavior that enable optimum design of the respective loads, such as processor, memory, I/O, disks, display, etc. [13]. The energy is supplied by two source converters: the adapter that interfaces to ac outlets worldwide or dc outlets in cars and airplanes, and the charger/discharger that assures optimum battery utilization. The power distribution system is then optimized independently, often using multiple bus converters with different voltages, e.g., 3.3, 5, or 19 V, depending on the power level. Although this may seem to be an overly complex approach, the overall energy consumption is reduced, the battery runtime and lifetime are increased, and the overall system weight and cost are actually smaller. It is also important to note that all the protection functions in the system (over- temperature, current, voltage) provided by the converters and their controls without thermo-mechanical breakers or fuses.

For this vision to be applied beyond small and autonomous power systems, future advancements in power electronics must go beyond components and converters themselves, addressing also the system-level integration of EPDS. The lack of standardized architectures and consistent system synthesis and integration methodologies, as well as the insufficient understanding and inability to quantify complex interactions and tradeoffs in these new power systems, represent major barriers to the widespread usage of power electronics converters. Future research in systems integration in power electronics thus may be focused on the following aspects:

- System architecture design and optimization;
- Energy flow control, protection, and power quality;
- System-oriented modeling of power converters.

This paper represents an attempt to illustrate some of the authors' thoughts on these research directions and their possible impact on the future electric power systems, especially in the presence of renewable energy sources. Several possible ac, dc, and hybrid EPDS architectures are discussed, followed by the description of static and dynamic operation of a hypothetical dc-bus-based EPDS in a future sustainable building. At the end, an example of terminal-behavioral modeling of a dc-dc converter for system-oriented analysis and design is presented. The discussion is illustrated by several large-signal average and small-signal simulations and an experimental result.

II. System Architectures

The architecture of an electric power system, including subsystem voltage and current ratings, is a major determinant for the system structural and thermal feasibility, safety, availability, size, weight, power and energy efficiency, reliability, and ultimately the cost of energy utilization. Although most of these are quantifiable physical variables, the sheer size of the design space in most applications, coupled with the uncertainty in the objective function, allows for numerous "equally optimum" system architecture solutions. Consequently, as in many other complex systems, the final choice is often a result of "religious wars" between different engineering traditions, situation which may further exacerbate in the future as electronic power converters pervade the developing EPDSs. However, if judiciously used, power converters – quite on the contrary – can enable the simplification of the design problem by separating the one-time complex system into a large number of smaller, well-defined, and easily optimized subsystems. The utilization of the energy sources and the power delivery to loads can then be optimized independently of the power distribution architecture, which is primarily determined by the type of application and the power level.

Contemporary trends, concerns about sustainability, and higher availability of smaller generating systems (i.e. solar cells, wind turbines) have opened new opportunities for electricity users to generate power on-site. The presence of distributed generation with associated electronic power converters, which are not controlled by the electric power utility operator has required fresh thinking about how the electric grid is built and operated, at least at the distribution level. The so-called microgrid is widely known and accepted concept that comprises energy storage and a larger number of generating units in order to get the most from the naturally available renewable energy sources while minimizing architectural changes and operational disruptions of the existing power grid [14], [15]. Based on these considerations, several candidates for EPDS architectures are illustrated below. The discussion is organized around the application in future sustainable residential buildings, but many ideas come from and could be applied in the other EPDS applications mentioned above.

AC Nanogrid

At extreme, the microgrid concept can be applied to residential electrical system at the low power level (10-100 kW) as shown in Fig. 2, when it may be termed a *nanogrid* [16], [17]. Combined with net-metering, communications, and remote control such nanogrids could become building blocks of a future "smart grid." Contemporary homes are envisioned to be energy sustainable and powered by a mix of renewable energy sources, together with utility grid. The sources would mainly include photovoltaic solar cells (PV), wind generators, micro-turbines, fuel cells, and local energy storage [18]. Plug-in Hybrid Electric Vehicles (PHEV) are also expected to become an inherent part of the future home [19].

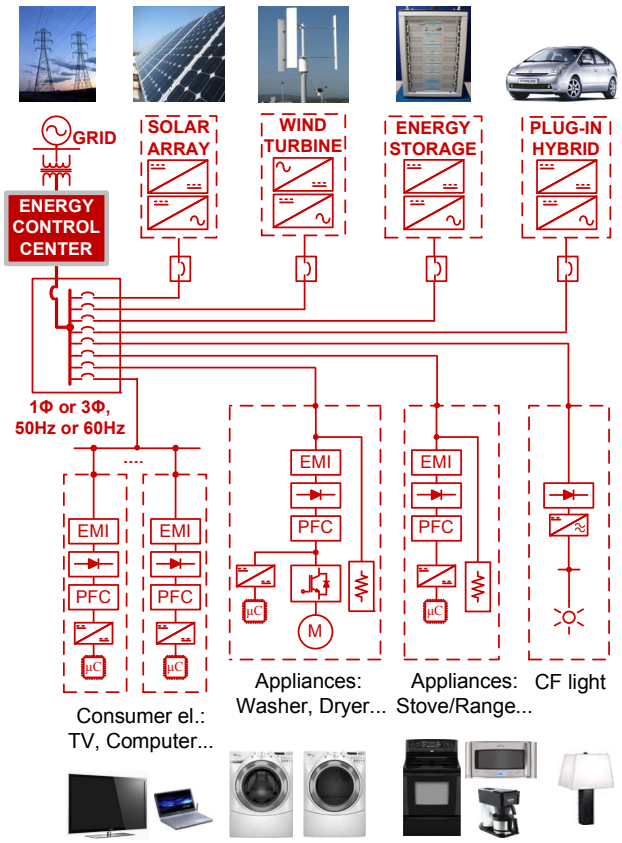

Fig. 2. A contemporary vision of "smart" nanogrid in residential home.

In the contemporary homes like the one shown in Fig. 2, the majority of the electrical household functions depend on the power electronics to convert electrical power into the form and amplitude required by the sources or loads. Through appropriate design of these devices and by operating them in a coordinated fashion, net residential fuel-based energy use can be reduced dramatically, while simultaneously increasing the perceived comfort levels in terms of lighting, temperature, water and air quality.

In a "smart grid" concept, the Energy Control Center (ECC) in Fig. 2 consists of a smart power meter and remotely operated (disconnect) breaker. ECC is able to communicate with the electric power utility operator for the energy trading purposes, and also acts as the data acquisition unit collecting and recording the power flow data not only from/towards the grid, but also from all the converters and "smart" appliances in the home. The major features that distinguish architecture of the shown electrical system in comparison with today's conservative home include the ECC, renewable energy generation, PHEV and/or local battery storage, as well as the ability to program and communicate with most of the system components ("distributed intelligence" capability) that is symbolized by the presence of many embedded microcomputers (µC) in Fig. 2.

Power converter for the PV is most commonly unidirectional two-stage converter featuring the step-up (boost) dc-dc converter stage and a single- or three-phase voltage source inverter stage for adequate interface with the utility grid [20]. New converters for small wind turbines are also two-stage power converters, comprising the three-phase PWM rectifier and a voltage source inverter. Energy storage and PHEV typically require bidirectional dc-ac converters for the optimal battery utilization on one side, and ac-line interface at the other.

Household loads more and more contain power electronics converters that optimize their operation and boost up the efficiency, as illustrated in Fig. 2. A modern washer, for example, features the variable speed drive that provides a maximal torque per current to the brushless motor, and thus more efficiently utilizes the energy compared with the conventional pole-changing induction motor often found in the older type of washers. Even once the biggest resistive load in a home, a stove, is being replaced with the one featuring induction heating and now becomes an electronic load to the system. Lower-power consumer electronics devices as TV, computer, audio and other portable ones, inherently comprise the power electronics circuits for operation, and boast with the "power aware" function enabled by it [21]. It is interesting to note that practically all electronic loads have two-stage power conversion, where the front-end converter consists of a rectifier, electromagnetic interference (EMI) filter, and often a power factor correction (PFC) circuit, as shown in Fig. 2.

Described system can work in two major modes of operation, grid connected and stand-alone mode, and perform two major transitions, islanding and synchronization. Together with the ECC, the bidirectional power converters from the PHEV and/or energy storage are responsible to isolate the home from the utility grid in the case of a fault or other abnormal grid conditions, perform the frequency and voltage regulation of the home ac-line in the stand-alone mode, and synchronize and reconnect the home to the utility grid without load power interruptions [22], [23]. This also presents the opportunity for demand-response operation while in the grid connected mode [19].

However, since the interface to the utility grid is still the ac-line itself, the described architecture does not yet completely resolve the coupled dynamics problem of the distributed generation and consumption. The "smart grid" concepts that imagine millions of individual sources and loads being controlled by the utility operator are unrealistic, while local interactions of these sources and loads will become intractable, especially whenever the local (neighborhood) generation is providing a significant amount of the local consumption. It seems that in future power systems with sizeable dispersed generation, the distribution systems cannot serve only for the load and source agglomeration, but must be hierarchically delegated a substantial authority over local voltage and frequency regulation in addition to the energy management.

A possible solution to this problem of "complexity curse" could the placement of a full-power bidirectional converter instead of the "smart" power meter in the Energy Control Center (ECC) in Fig. 2. In that case, the whole nanogrid of the building is seen by the utility grid as a single electronic load/source, dynamically independent of the grid but dispat-

chable by the utility operator. The ECC is entrusted with the operation of the local renewable generation, load shedding, utilization of the static or mobile battery (PHEV) energy and other power management functions, as well as nanogrid stabilization and advanced, active islanding in the event of outages or other low frequency disturbances on the utility side. In the proposed hierarchical grid architecture, the nanogrids are fully dynamically decoupled from grid through ECC, so that their internal architecture is completely independent and can have different voltage, phase, and even frequency, from dc to kilohertz.

DC Nanogrid

Once the nanogrid is dynamically separated from the rest of the grid, it is easy to envision that the future building electric systems could be based on a dc nanogrid, as shown in Fig. 3. Compared to the ac nanogrid architecture in Fig. 2, dc nanogrid brings many advantages, starting with fewer power converters, higher overall system efficiency, and easier interface of renewable energy sources to a dc system. There are no frequency stability and reactive power issues, and no skin effect and ac losses. What is more, the consumer electronics, electronic ballasts, LED lighting, and variable speed motor drives can be more conveniently powered by dc.

The future home dc nanogrid is envisioned to have two dc voltage levels: a high-voltage (380 V) dc bus powering HVAC, kitchen loads, and other major home appliances, and a multitude of low-voltage (48 V) dc buses powering small tabletop appliances, computer and entertainment systems, and LED lighting. The 380 V dc level is chosen to match the industry-standard intermediate dc voltage in consumer electronics with the PFC circuit at the input, so that conversion from ac to dc would involve only bypassing (or eliminating) the front-end rectifier and PFC in most contemporary appliances. The 48 V dc level coincides with the standard telecom voltage to facilitate adoption, increase efficiency, and provide enhanced safety when handling small appliances, while enabling aesthetically attractive designs with exposed electrical-structural elements. Beside the dc distribution systems already proposed for commercial and residential applications [24]-[29], similar dc power distribution systems are currently being considered for datacom centers in Japan, Europe, and USA [30]-[32], and are also being contemplated for PHEVs and aircraft power systems [33], [34]. Several manufacturers already have on the market high power-density bus control modules (BCMs) that supply 48 V from 380 V and are intended for these applications [35], [36].

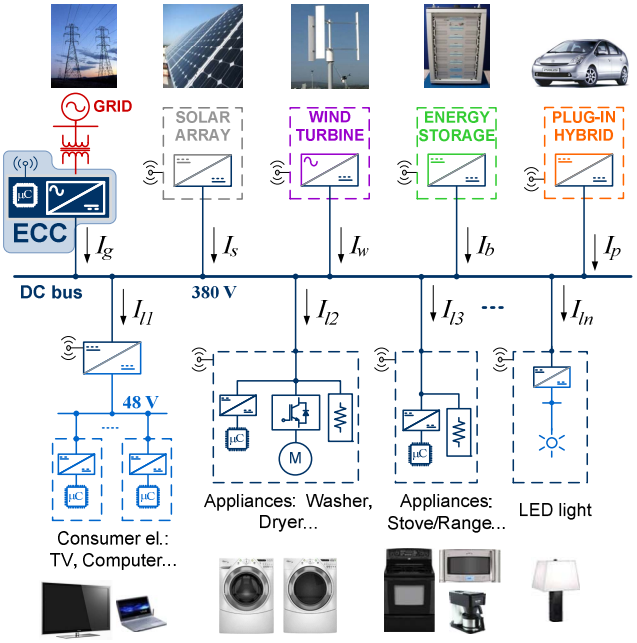

Fig. 3. A dc-based nanogrid in a future home.

In higher voltage dc systems, fault current interruption is of particular concern. However, in the proposed nanogrid architecture all power is fed from electronic power converters that are controllable and can provide active current limiting, thus reducing the need for electromechanical protection devices. The system could be even completely breakerless if all the source converter topologies comprise serial semiconductor switches which fail "open" in the case of abnormal failure. This would also eliminate the need for significant over-sizing of the wiring and upstream converters that is traditionally used to ensure safe clearing of the electromechanical breakers in the case of faults. Therefore, such nanogrids may be able to provide increased energy efficiency, power density, and reliability, at possibly lower installation and operation costs. However, further research is needed on the development of physics-based models that quantitatively relate these variables while accurately describing system dynamical behavior, before new nanogrid architectures could be truly optimized and the described tradeoffs justified.

Intergrid

The proposed ac and dc architectures have several main distinguishing features:

1. At least a minimal level of local energy generation and/or storage;
2. Interface(s) to the higher-level system exclusively through bidirectional electronic power converter(s);
3. Ability to operate in islanded mode, at least during transients;
4. All energy sources and storage connected through electronic power converters;
5. Most loads connected through electronic power converters;
6. Extensive communication and control capabilities, both internally and externally;
7. Most (possibly all) protection and reconfiguration functions provided by the electronic power converters, without the use of thermo-mechanical switchgear;
8. Step-up/down and isolation functions provided by the electronic power converters without the use of low-frequency transformers.

Although all of these features could be achieved either with ac or dc, the presence of the last two eliminates any natural advantage of the low-frequency ac systems, while all the fea-

tures could be achieved more efficiently in a dc system. There is also a preference for linear bus structures instead of radial ones in order to reduce wiring and simplify system construction and maintenance.

Similar architectures, for example, can be found in the dc-zonal power distribution system for future ships, [37], [38], where generation and propulsion are decoupled so that energy sources can be distributed as required by other considerations. The system flexibility and reconfiguration capacity are maximized by using a dual dc-bus feeder structure, and by sectionalizing loads into groups (zones) distributed along the ship, which are fed from redundant "zone distribution converters".

Power-electronics-interfaced high-voltage dc (HVDC) transmission has gained significant interest due to the increasing needs and socio-economical benefits of underground and underwater cable transmission, [39]-[41]. Although at this power level the function of the converters is clear, system architectures to perform these tasks are under continuous development as the technology improves.

It is then possible to contemplate that the proposed architectural concept of the nanogrid could be extended hierarchically, so that a number of such semi-autonomous nanogrids with nECCs are combined to form a bigger microgrid system, which in-turn is interfaced to a higher-level distribution through a substation µECC, and so on, as shown in Fig. 4. The resulting system is a hybrid mix of ac and dc architectures comprising …, pico-, nano-, micro-, …, sub-grids that are dynamically decoupled and hierarchically *inter*connected to form a novel electric power *grid* structure: the *intergrid*.

AC and dc nanogrids in Fig. 4 correspond to the systems shown in Figs. 2 and 3, respectively. The PHEV electrical system with its bidirectional charger/discharger, on-board batteries, and the generator powered by internal combustion engine, as well as numerous on-board electronic loads, has all eight features listed above, and hence could be considered a miniature "picogrid". Numerous nanogrids can be connected to a distribution network, but they are considered to comprise a microgrid only if the network is connected to the next upstream level through one or more bidirectional µECCs.

The ECCs that interconnect various subgrids are not only bidirectional power converters, but actually "energy routers" that provide load and source aggregation, data acquisition and agglomeration, command communication and distribution, and have sufficient authority to enable hierarchical distributed control of the whole grid. Every ECC is capable to communicate with all of the downstream components in the subgrid as well as with the next level upstream ECC, in order to fully utilize and optimize operation of the particular subsystem, and consequently influence the overall operation of the intergrid.

Containing a bidirectional converter, an ECC can control the continuous energy flow into and out of the subgrid, and can perform intentional or unintentional islanding of the subgrid depending of the fault nature in the upstream system. By utilizing power electronics converters for all distributed generation – including numerous renewable sources and storage

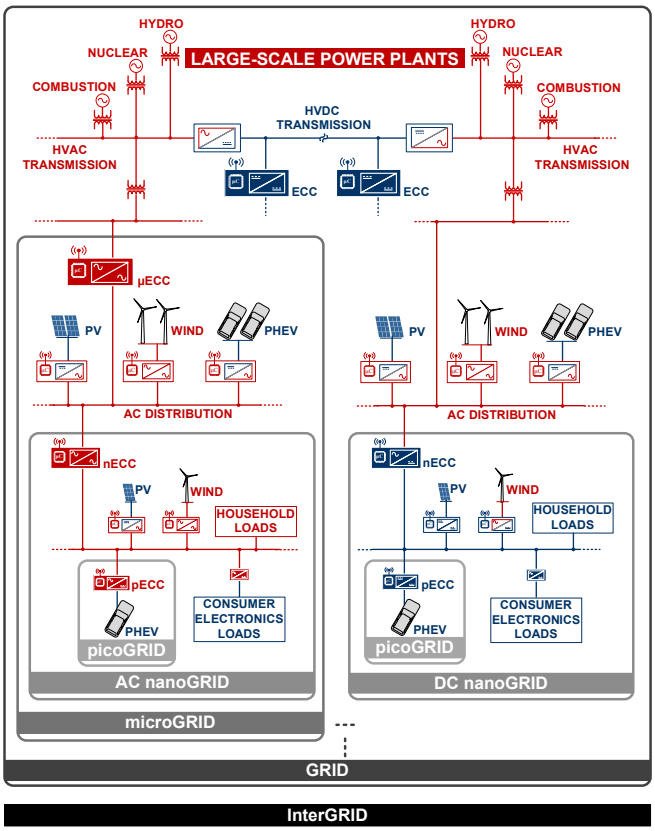

Fig. 4. Conceptual intergrid system structured as a hierarchically interconnected hybrid mix of ac and dc sub-grids.

facilities – it is possible to continue operating the subgrid during brief and long upstream power interruptions. With emerging advanced control algorithms, the PV, wind-turbine, and other source converters can regulate the bus voltage (and frequency for ac systems) and share the load current even in the weak-grid and stand-alone modes of operation, instead of only operating in the maximum power point tracking (MPPT) mode [42]. Obviously, this requires local demand-side management in order to balance the generation and consumption in the islanded subgrid, which is enabled by the presence of remotely controllable and fast point-of-load (POL) electronic power converters. Although most of the issues are very similar to the ones existing in the power grid today, they are much less complex and could easily be automated when dealing with tens of sources and hundreds of loads at every hierarchical level, instead of dealing simultaneously with thousands of sources and millions of loads at the whole grid level.

Furthermore, the contemplated intergrid concept is compatible with the existing grid and could be introduced gradually. New sustainable buildings, datacom centers, commercial and industrial areas, renewable and distributed generation facilities, small- and large-scale energy storage installations, as well as new power distribution in highly populated and congested areas (with no available right-of-way) could all be economically implemented as ac or dc nanogrids and microgrids. These subgrids become dispatchable generation and load resources that can respond very fast to the commands

from the power system operator and thus can participate in grid stabilization, voltage and frequency control, real-time pricing, and become an inherent part of the everyday grid operation. At the other end, the existing congestions in the transmission system and the rising concerns for the grid stability with the increased penetration of renewable generation are increasingly being alleviated by the construction of new HVDC transmission lines, which will enable decoupling of the existing megagrid into many smaller and better controllable asynchronous grids. By utilizing the fast dynamic response of electronic power converters, the energy could be easily rerouted between different subgrids, which can significantly reduce the need for the spinning reserve and facilitate the use of peaking power plants to compensate for the fluctuations in renewable energy generation.

Although the use of dc architectures facilitates and simplifies the dynamic decoupling of the interconnected subgrids, and more importantly improves the overall energy efficiency of the system, the disadvantage can be expensive infrastructure and protection components, as well as the fact that large scale dc system implementation is not mature enough and still requires intensive research before standards can be developed and industry acceptance achieved.

III. Static Operation of the Nanogrid

Although a generic intergrid concept has been proposed and discussed in the previous section, the remainder of this paper will stay focused on the dc-based nanogrid system at the residential level shown in Fig. 3, which is being experimentally implemented in the CPES labs. The static operation of that system is presented below.

The concept accepted for the voltage regulation in the nanogrid system is the droop control based on the dc-bus signaling technique [43], [44]. The qualitative sketches of the dc output V-I characteristics for all the energy source converters in Fig. 3 are shown in the Fig. 5. The nominal voltage of the dc bus is 380 V, but the operating voltage range of the bus is chosen to be between 360 V and 400 V to allow for power sharing and voltage regulation using the droop control. All converters are programmed to turn off after the voltage at the converter terminals stays below 360 V for some predetermined time, and to turn off instantaneously if the voltage exceeds 400 V by some margin.

Starting with the bidirectional grid interface converter, its V-I curve is shown at the top-left in Fig. 5. In the first quadrant of the V-I plane this converter is taking energy from the grid when the current I_g shown in the Fig. 3 is positive, while in the second quadrant it is sourcing energy back to the grid. The V-axis intercept is 380 V, which is the nominal bus voltage, and the droop slope (virtual dc output resistance), R_{gd}, is a design parameter. If the converter output is overloaded or even shorted in the first quadrant, the converter limits the output current to I_g^D in Fig. 5. The "V-I knee" where the converter changes its mode of operation from the voltage droop mode to the current regulation mode is chosen to be 370 V to

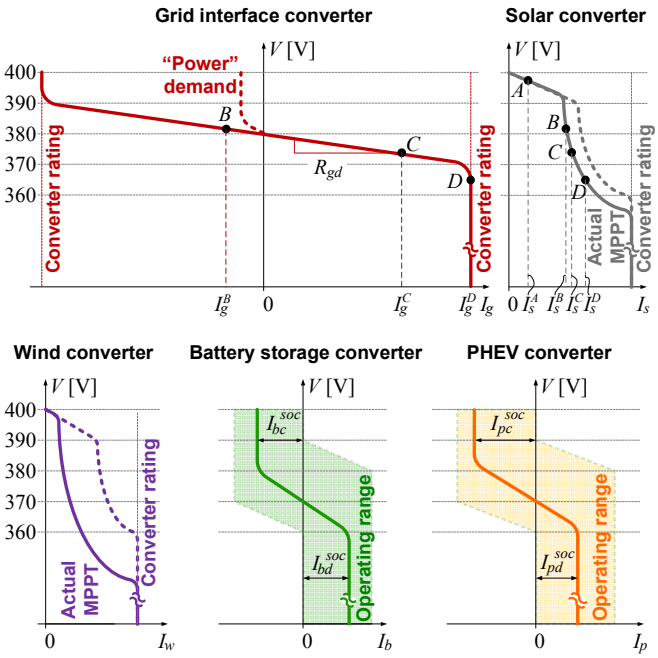

Fig. 5. Qualitative static V-I characteristics of the energy sources in dc nanogrid from Fig. 3.

allow for the energy storage converters to start regulating the dc bus when the grid-interface converter rating is exceeded. In the second quadrant, the converter to exhibits the symmetrical current limit due to the assumed same rating in the grid-sourcing mode. If the operator of the power system to which the nanogrid is connected requests from the ECC a specific amount of power that is less than the converter rating, the converter can reprogram its V-I characteristic in the second quadrant to limit the current to a value that corresponds to the demanded power, as represented by the dotted line.

The V-I characteristic of the solar converter is shown at the top-right in Fig. 5. Since the solar PV can only generate, the converter output current, I_s, is always positive in Fig. 3 and Fig. 5. The dotted line represents the maximum capabilities of the PV system that correspond to the maximum solar insolation. For very light loads, when the voltage at the converter terminals is between 400 V and 390 V, this converter can regulate the bus by operating in the voltage droop mode. Once it reaches the maximum available power, it continues to operate in the MPPT mode as a constant power source. The converter absolute current rating is shown as the vertical line defining the maximum current limit. The actual MPPT curve at some moment of time is shown as the solid line; it constantly changes depending on the available solar insolation at the particular moment. It can be noticed that "V-I knee" in this case is not exactly at the 390 V, but slightly higher to allow keeping the same predefined droop slope for all insolation conditions.

The wind turbine converter V-I curve in Fig. 5 has the same characteristics as the solar one. The actual MPPT depends on the wind speed and can happen anywhere between the zero converter output current and the absolute current

limit. The V-axis intercept and the droop slope are system design parameters and they are selected for both the solar and the wind converter so that the voltage droop range falls between 400 V and 390 V. In this way, the renewable generation (when available) is given the highest priority in the energy utilization sense, i.e. the solar and wind converters are not operating in the MPPT mode only when the grid is not available and the total load on the nanogrid is smaller than the maximum available renewable power.

The battery charge/discharge converter has slightly different properties then previously explained converters in a sense of the droop characteristic adaptability. In Fig. 5, the battery converter V-I curve can be anywhere within the green shaded area called the operating range. The very right and very left vertical edge of this region represent the absolute capabilities of the converter itself. Current I_b in Fig. 3 and Fig. 5 is negative while the battery is charging. The vertical lines of the static characteristic in the first and second quadrant of the V-I plane are determined with the battery state of charge (SOC), where I_{bc}^{soc} and I_{bd}^{soc} represent the maximum allowed charging or discharging currents, which could but do not have to be the same. The battery converter receives the information about the SOC and the desired charging/discharging profile from the battery monitoring system and sets the current limits accordingly.

The droop part of the battery charger/discharger characteristic is set by the nanogrid energy control center (nECC in Fig. 3) according to a preprogrammed *optimal energy utilization algorithm*. The algorithm is based on the history of the battery SOC and could take into account the instantaneous and historical price of energy that could be drawn from or supplied to the utility grid, as well as the long- and short-term histories of the local renewable energy generation and the nanogrid load profiles. The nECC then can make a decision on the battery energy utilization to meet a predetermined optimization goal, and instruct the battery converter to adjust the V-axis intercept and the droop slope accordingly.

If the optimization of energy use is not active, the battery charger/discharger static characteristic is in the default position shown in Fig. 5. It assures that the battery is being charged whenever the nanogrid load demand is smaller than the total generation capacity. Only if the system bus voltage drops below 370 V – representing the case when the demand in the system is high and all of the non-storage sources are exhausted (in the current limit) – the converter provides voltage droop regulation of the dc bus in the range of 360-370 V. If the demand increases even more, the nECC could initiate a *load shedding algorithm* to prevent the dc bus voltage from dropping below 360 V, which otherwise would cause the bus voltage collapse and system shutdown.

The PHEV bidirectional converter is actually a part of the energy control center in the vehicle picogrid (pECC) as shown in Fig. 4. Essentially, when the car is connected to the nanogrid, the converter has the same properties as the battery charge/discharge converter described above, and its static characteristic is illustrated at the bottom-right of Fig. 5. However, the energy optimization algorithm may in this case also take into account the past and intended use of the vehicle, and the final setting of the V-I curve parameters could be resolved through automatic, real-time, negotiation between the nECC and the pECC.

In order to simplify the explanation of the proposed static load sharing between various sources in the nanogrid, all voltage drops on the dc bus cable impedances have been neglected. Although this is generally not true in distributed architectures, the assumption does not cause significant errors in dc systems if the droop regulation voltage range (~20 V in Fig. 5) is much larger than the voltage drops on distribution cables. Under these circumstances, the static characteristics in Fig. 5 are used to find the dc operating point of the nanogrid in Fig. 3 together with the following two conditions:

- all sources and loads share the same bus voltage; (1)
- source and load currents balance each other,

$$I_g + I_s + I_w + I_b + I_p = I_{l1} + I_{l2} + I_{l3} + \cdots + I_{ln} = I_L \quad (2)$$

For simplified explanation of the nanogrid static operation consider an example when the system comprises only two sources, the grid interface converter with the source current I_g and the solar converter with the source current I_s, and one equivalent load, I_L. For the start, it will be assumed that the grid is not present, and the system (now only solar and the load) works in the islanded mode with negligible change in the solar irradiation. If the load demand is small, say I_l^A in Fig. 5, the solar converter alone provides the total load current, $I_s^A = I_l^A$, and regulates the bus voltage to slightly below 400 V (point *A* in Fig. 5).

Assuming that the load doesn't change, let us now consider the condition after the nanogrid is reconnected to the utility grid through the grid interface converter. The new equilibrium point moves to *B* in Fig. 5 at the voltage slightly higher than 380 V, where the solar converter now operates in the MPPT mode, while the grid converter regulates the bus. Because the load current remained small, $I_l^B = I_l^A$, the grid converter current,

$$I_g^B = I_l^B - I_s^B \ , \quad (3)$$

becomes negative and is fed back to the utility. When the load current is increased to a much higher level, I_l^C, and system moves to a new equilibrium at the bus voltage between 370 V and 380 V (point *C* in Fig. 5), where the grid interface converter now feeds most of the energy from utility grid. Solar converter output current changes only slightly due to the fact that it operates in the MPPT mode with the high output impedance.

If the load is eventually increased even more, the system can be forced to the point *D* in Fig. 5, at the bus voltage below 370 V. At this point both sources operate in high output impedance modes (current limiting and MPPT), which is usually unstable because the voltage will decrease further with even a slight increase of the load current, and conse-

quently source converters will go offline after the bus voltage drops below 360 V level.

Using the conditions (1) and (2), the nanogrid operating points could be found in a similar manner for any combination of the energy sources with the static characteristics in Fig. 5. However, if the dynamic properties of the sources and loads, as well as the bus cable impedance, are taken into account the system transient behavior can become more complex, as will be illustrated in the next section.

IV. Power Flow Control and Stability

The key enabling concept for EPDS is the electronic power-flow control and protection within power systems, where power converters are not only used for voltage and frequency conversion, but also for power flow control, monitoring, diagnostics, and fault protection. A converter for instance, with proper current and voltage limits, is capable of rerouting the energy more orderly during a transient than the traditional system based on mechanical switchgear. In order to illustrate better the overall performance, stability and protection features of the nanogrid system in the Fig. 3, a simplified dynamic simulation and analysis of the system behavior will be presented next.

System Modeling

A minimal relevant system that represents nanogrid from Fig. 3 is shown in Fig. 6. It consists of two sources, the bidirectional grid interface converter and the solar PV converter, and two generic loads with point-of-load (POL) converters. For further simplification, all system wiring is represented with a single RLC circuit placed between the sources and the loads. The dynamic behavior of that system is then analyzed by using large-signal average models of the converters and conducting large-signal time-domain and small-signal frequency-domain simulations. Due to the obvious oversimplifications, the results are more of a qualitative nature and can serve only as guidelines for future research directions.

In the analyzed system in Fig. 6, the grid interface converter is a 10 kW two-stage bidirectional converter: a single-phase full-bridge ac-dc PWM rectifier/inverter in series with a dc-dc PWM converter. As shown in [45], such converter can achieve bidirectional power flow control and dc-bus voltage regulation in addition to the substantial reduction of the dc-link capacitor for higher power density. For the purposes of the simulation here, the grid interface converter is modeled in Saber [46] using detailed average model, including input and output current and voltage control loops, which also implement the static behavior shown in the Fig. 5 with the current limit of around 28 A and the voltage droop slope of $R_{gd} \approx 0.4\ \Omega$. The 380 V dc bus voltage-loop bandwidth is around 1 kHz.

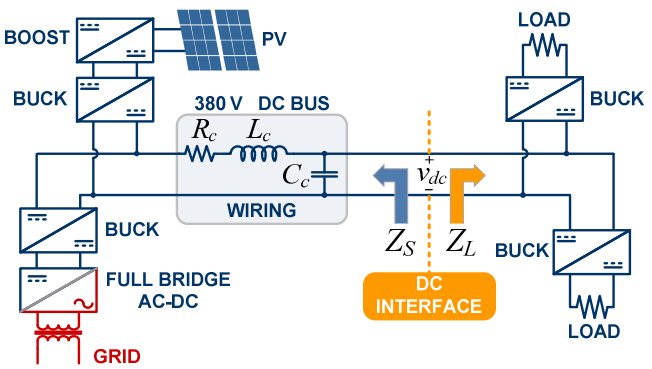

Fig. 6. Minimal relevant structure for analysis of the nanogrid system.

The other representative source converter for the dynamic analysis is chosen as a 5 kW solar converter. It is a unidirectional two-stage converter comprising the front-end boost in series with a dc bus buck regulator, which provides for good energy efficiency as well as excellent bus regulation and system protection. Average models are used for the analysis, including an MPPT controller in the boost stage, and the output current and voltage control in the buck stage to implement the static behavior shown in the Fig. 5 with the current limit of around 15 A, the voltage droop slope of around 0.7 Ω, and the voltage-loop bandwidth of around 1 kHz.

The POL converters are represented using simple average models of unidirectional buck converters with output current and voltage control. The high-gain voltage loop bandwidth is around 15 kHz making the POLs behave like constant power loads (CPL) on the dc bus. The load variations are simulated with variable resistors at the POL outputs. To further simplify analysis, the power cables and all differential-mode EMI filters that are distributed around the system outside of the converter control loops are modeled with the single RLC circuit shown in Fig. 6 with the following values:

$$R_c = 0.1\,\Omega, \quad L_c = 10\,\mu\text{H}, \quad C_c = 30\,\mu\text{F}\ . \tag{4}$$

Large-Signal Transient Analysis

Using the described dynamic models, the large-signal transient behavior of the sample system in Fig. 6 was simulated in Saber to illustrate some of the transitions between the operating points *A*…*D* in Fig. 5, and the results are summarized in Fig. 7. In the case that the nanogrid is supplied only by the solar energy without the grid, Fig. 7.a shows the dc bus voltage transient when the load (and source) current is increased to about 10 A, which corresponds to the operating point *A* in Fig. 5. It can be seen that the solar converter provides very effective droop regulation of the dc bus voltage even for the very fast step increase of the CPL load.

When both the grid and solar are present, it could be expected that the solar converter works all the time in the MPPT mode, while the grid interface converter provides the droop regulation of the dc bus voltage. This condition is illustrated by the simulation results in Fig. 7.b, where the CPL converters ramp the power demand from few kilowatts to over 13 kW, corresponding to the change of operating point from *B* to *C* in Fig. 5. At the beginning, while the load current is small, most of the energy sourced by the solar converter operating in the MPPT mode is being fed back to the ac grid, as can be observed from the bottom two plots in Fig. 7.b. As the load increases, the grid interface converter continues to regulate the dc bus voltage very smoothly in the droop control

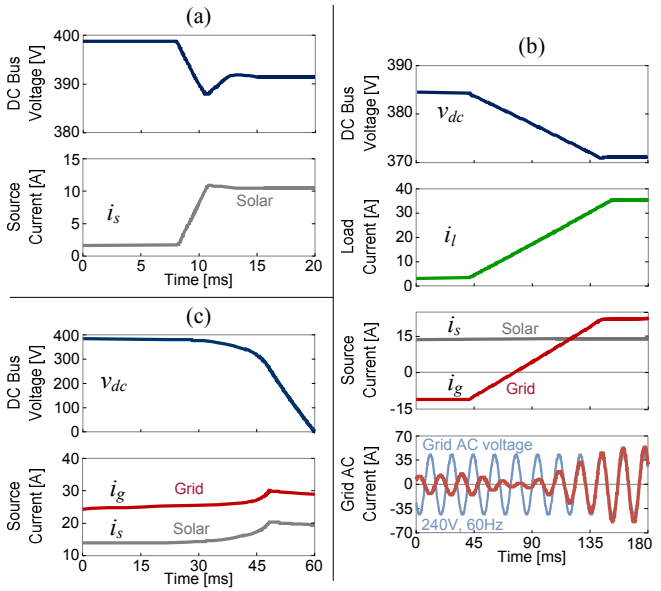

Fig. 7. Time-domain simulation waveforms for the system in Fig. 6 under large-signal transitions between different operating points in Fig. 5: a) Move to *A* in islanded mode, b) Transient *B*→*C*, c) Transient *C*→*D*.

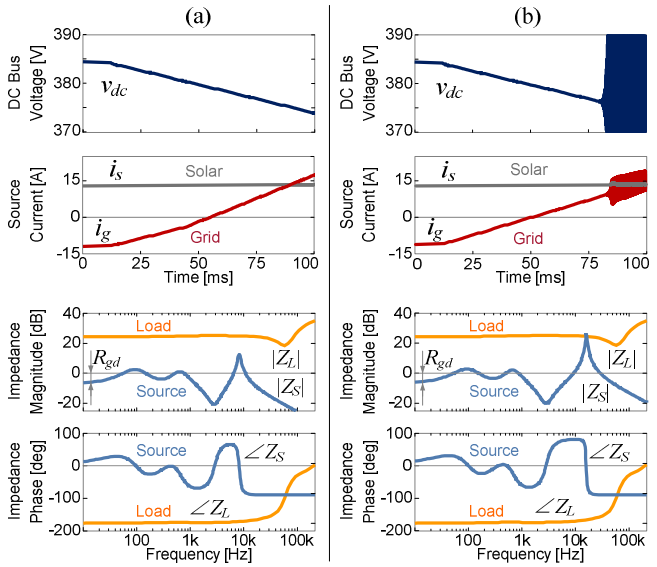

Fig. 8. Large-signal time domain and small-signal frequency domain results of stability analysis for the system in Fig. 6 showing: a) Stable operation with C_c = 30 µF, b) Unstable operation with C_c = 8 µF.

mode, even as its ac and dc currents reverse the direction and its operating point moves from the second to the first quadrant of the V-I curve in Fig. 5.

The simulation results that illustrate the nanogrid behavior in overload are shown in Fig. 7.c. If the CPL power is kept increasing, the system operating point will move from *C* to *D* in Fig. 5, when both source converters will run into current limit mode. Although the load demand continues to increase, the source converters protect the system by reducing the dc bus voltage very fast, thus limiting the bus current to slightly more than rated even when the voltage drops to zero (dead-short). After some preset time, the system then can be shut down in an orderly and safe manner.

Stability Analysis

The system static/transient behavior illustrated in Fig. 7 reflects the system behavior in a well-designed case. This includes the selection of relatively large distributed capacitors on dc bus, which are modeled by a single capacitor C_c in Fig. 6 with the value given in (4). This provides for passive decoupling of the small-signal dynamic interaction between the sources and the constant power loads at the "DC Interface" in Fig. 6. However, a desire to reduce the size of the energy storage components, calls for attention due to the concern for the system stability. Fig. 8 illustrates the stability study of the sample dc nanogrid system with different bus capacitors. Time domain simulation results in Fig. 8.a are essentially zoomed-in waveforms of the dc bus voltage and source currents for the transition from operating point B to A shown in Fig. 7.b. The time domain waveforms in Fig. 8.b are obtained under identical operating conditions, except that the bus capacitor C_c is reduced from 30 µF to 8 µF. As can be observed, the system becomes unstable when the CPL converters' power increases to around 7 kW. The oscillations are close to the dc bus resonant frequency, $(2\pi\sqrt{L_c C_c})^{-1}$.

The cause of instability can be investigated by observing the source output impedance Z_S, and the load input impedance Z_L at the dc interface in Fig. 6. If Z_L/Z_S is far away from the critical −1 point, the system is stable; otherwise the system will be unstable under some power level condition. The Bode-plots of the impedances at the dc interface were obtained using small-signal (AC) analysis of the average system model shown in Fig. 6 at the operating point of 7 kW, and are also shown in Fig. 8. The load input impedance clearly shows the CPL characteristic ($\angle Z_L \approx -180°$) up to tens of kilohertz. Under the stable case shown in Fig. 8.a, the magnitude of Z_S is lower than Z_L with sufficient margin, while in the case shown in Fig. 8.b, the dc bus resonant peak touches Z_L at 18 kHz, leading to the unstable oscillations.

The previous analysis illustrates the importance of the interconnect interface impedance matching for the system-level design and stability prediction. Therefore, it is very necessary to obtain the accurate terminal characteristics of converters, especially if the internal structure is unknown.

V. System Oriented DC-DC Converter Modeling

Considerable work has been done up to now on modeling and capturing the system interactions at fundamental and low frequency, e.g. power flow and small-signal stability and interactions between converter modules and passive filters for dc distributed power systems [47]-[49]; studying the effect of converter-generated switching harmonics (medium frequency range) on system resonances, and power quality in ac and dc systems [50]-[51].

However, system-level design is significantly hampered by the fact that system engineers rarely have access to all the

information required to model all converters, and in fact they will usually know only the input and output voltages and power ratings of the components. This is common in systems built by integrating power converters, filters, protection devices, and loads designed and manufactured by different companies, which normally provide little or no information about the design and internal structure of their products. Consequently, the design and construction of these systems finally relies entirely on the experience of engineers, and the testing of the final system under multiple operating modes.

In order to alleviate these problems, terminal-behavioral modeling of converters became an attractive topic in addressing not only low-frequency dynamic behavior of the converters [52]-[54], but also the high frequency EMI [55], [56] as well as efficiency, system stability, inrush current, protections, start-up and remote on-off control [57].

Low-frequency terminal-behavioral models are usually derived directly from the final hardware products using a network analyzer to measure frequency response characteristics of interest, which are then processed and used to build a two-port (g-parameter) network equivalent circuit shown in the Fig. 9. The converter input-output relationships are hence given by:

$$\begin{bmatrix} v_2 \\ i_1 \end{bmatrix} = \begin{bmatrix} G_o(s) & -Z_o(s) \\ Y_i(s) & H_i(s) \end{bmatrix} \cdot \begin{bmatrix} v_1 \\ i_2 \end{bmatrix}. \tag{5}$$

The fundamental assumption in this modeling approach is that the converters are "mildly nonlinear," i.e. that the nonlinear and dynamic components of the converter behavior could be separated. In that case, (5) is a small-signal model around an operating point, while parameters of the four transfer functions can depend in a nonlinear way on the slowly changing operating point.

Procedure for obtaining the terminal-behavioral model consists of two separate sets of measurements on the converter working at desired operating point, as shown in Fig. 9. It is very important to assure that the operating conditions of the converter under test do not change substantially during and between the two tests. It should be noted that in order to assure the desired operating point, all the measurements are conducted with the "terminated" converter, meaning they are not fully decoupled from the source and the load used in the measurement setup. Hence, the dynamic properties of the load and source are inherently contained in the *m*easured frequency response characteristics and to distinguish them from (5), they are denoted with the subscript letter *m*.

From the first set of measurements, when perturbation is performed on the input side of the converter under test (Setup 1 in Fig. 9), three *m*easured transfer functions can be obtained: audio-susceptibility G_{om}, input admittance Y_{im} and transconductance T_{gm}:

$$G_{om} = \frac{\tilde{v}_2'}{\tilde{v}_1'}, \quad Y_{im} = \frac{\tilde{i}_{1R}'}{\tilde{v}_1'} \quad \text{and} \quad T_{gm} = \frac{\tilde{i}_2'}{\tilde{v}_1'}. \tag{6}$$

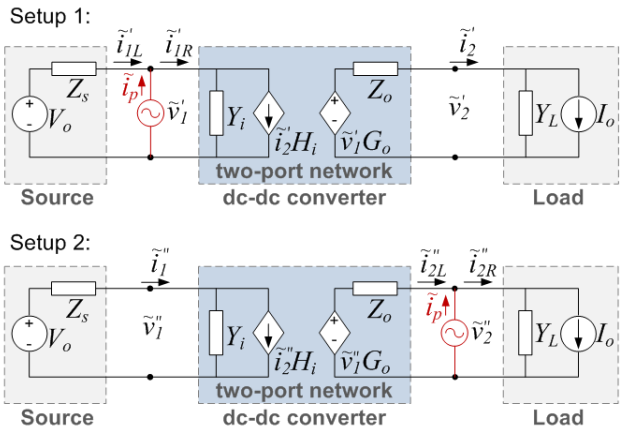

Fig. 9. Measurement setup for terminal characterization of a dc-dc converter.

The next set of measurements (Setup 2 in Fig. 9) is performed when the converter output is perturbed, so that another three frequency response characteristics can be obtained: back-current gain H_{im}, output impedance Z_{om} and transresistance T_{rm}:

$$H_{im} = \frac{\tilde{i}_1''}{\tilde{i}_{2L}''}, \quad Z_{om} = \frac{\tilde{v}_2''}{\tilde{i}_{2L}''} \quad \text{and} \quad T_{rm} = \frac{\tilde{v}_1''}{\tilde{i}_{2L}''}. \tag{7}$$

In order to decouple source and load dynamics from the measured characteristics, the transformation

$$\begin{bmatrix} G_o \\ Y_i \\ Z_o \\ H_i \end{bmatrix} = \begin{bmatrix} 1 & 0 & -T_{gm} & 0 \\ 0 & 1 & 0 & T_{gm} \\ T_{rm} & 0 & -1 & 0 \\ 0 & T_{rm} & 0 & 1 \end{bmatrix}^{-1} \cdot \begin{bmatrix} G_{om} \\ Y_{im} \\ Z_{om} \\ H_{im} \end{bmatrix} \tag{8}$$

has to be used to solve for the un-terminated transfer functions in the model (5). It is interesting to notice that the measured transconductance and transresistance appear only in the decoupling matrix in (8). The same procedure can be applied to both, closed-loop and open-loop converters, assuming that they behave linearly for small perturbations, $\tilde{\imath}_p$.

As an example, two-port terminal characterization is performed on the switching model simulations of the 380 V to 48 V unregulated buck converter shown in the Fig. 10. Switching frequency is 38 kHz, and all circuit parameters are given in the figure. In the Fig. 11, four frequency response characteristics defined in (5) are plotted up to the half of the switching frequency. Blue curves are obtained from simulations by directly applying the measurement procedure illustrated in Fig. 9, and represent the first two frequency characteristics from (6) and first two from (7). The red curves represent the decoupled frequency response characteristics obtained by using (8).

To verify the procedure, time domain-switching model simulation of the source-converter-load system from Fig. 10 has been performed, and the results are shown in the Fig. 12 colored in gray. In the same figure, the terminal-behavioral model simulation results are shown plotted in red color over

the switching model dynamic response of the four terminal variables. The evident degree of matching indicates a possibility of using the terminal-behavioral models in the system-level simulations and analysis.

This modeling approach can be readily used for extracting dynamics of linear or "mildly" non-linear converters. A closed-loop regulated buck converter would represent a non-linear system exhibiting "constant power" characteristics at the input. In that case, the dc gain of the reverse current transfer function, $H_i(s)$, would be given by

$$H_i(0) = \frac{V_{2\text{ref}}}{\eta(V_1, I_2)\cdot V_1} \quad \text{for} \quad V_{1\min} < V_1 < V_{1\max}, \qquad (9)$$

where η is the converter efficiency, and the uppercase symbols denote steady-state (long-term average) values of the input and output variables. It remains to be investigated if the multiplicative amalgamation of the models (5) and (9) could produce meaningful results. It remains to be explored if there is a consistent methodology for combining the small-signal characteristics (5) of a converter with its large-signal static characteristics of the form shown in Fig. 5. This could be immensely useful for low-frequency analysis and design of complex EPDSs such as the proposed *intergrid*.

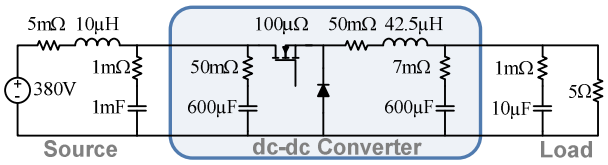

Fig. 10. Buck converter used for verification of terminal-behavioral model.

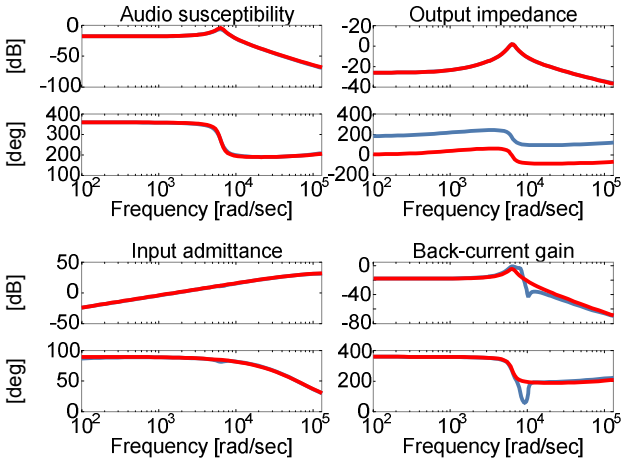

Fig. 11. **Blue**: measured, terminated; **red**: un-terminated transfer functions.

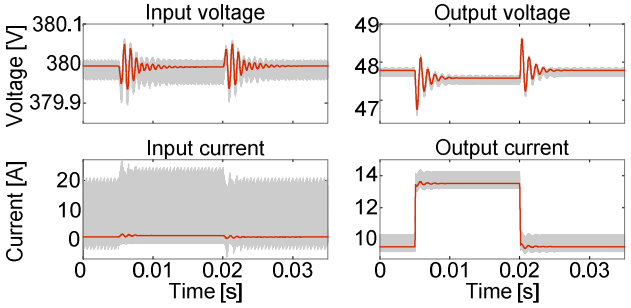

Fig. 12. Time domain simulation of the converter from Fig. 11: **Gray:** switching model; **red:** terminal-behavioral model (5)

VI. Conclusion

Past advancements in integration of power electronics components and converters are now enabling major improvements in the power density, reliability, energy efficiency, and cost effectiveness of electrical power systems. These improvements are already evident in the low power systems for portable equipment and are increasingly affecting new designs for autonomous power systems in vehicles, airplanes, ships, future homes, microgrids and the whole electric power system. Further penetration will strongly depend on the progress in our ability to model, understand, design and dynamically control desired and undesired subsystem interactions in the new, electronic power distribution systems ranging from a few watts to the hundreds of gigawatts.

References

[1] T. G. Wilson Sr., "The evolution of power electronics," *IEEE Trans. Power Elec.*, vol. 15, no. 3, pp. 439-446, May 2000.

[2] F. Blaabjerg, Z. Chen, and S. B. Kjaer, "Power electronics as efficient interface in dispersed power generation systems," *IEEE Trans. Power Electron.*, vol. 19, no. 5, pp. 1184-1194, Sep. 2004.

[3] R. Strzelecki, G. Benysek (editors), *Power electronics in smart electrical energy networks*, London: Springer-Verlag Ltd., 2008.

[4] N. Osifchin, "A telecommunications buildings: power infrastructure in a new era of public networking," *IEEE INTELEC 2000*, pp. 1-7.

[5] A. Emadi, Y. J. Lee, K. Rajashekara, "Power electronics and motor drives in electric, hybrid electric, and plug-in hybrid electric vehicles," *IEEE Trans. Industrial Electron.*, vol. 55, no. 6, pp. 2237-2245, Sep. 2008.

[6] J. A. Rosero, J. A. Ortega, E. Aldabas, and L. Romeral, "Moving towards a more electric aircraft," *IEEE Aerosp. Electron. Syst. Mag.*, vol. 22, no. 3, pp. 3–9, Mar. 2007.

[7] T. Ericsen, Y. Khersonsky, and P. K. Steimer, "PEBB concept applications in high power electronics converters," *Proc. IEEE PESC*, pp. 2284- 2289, Sep. 2005.

[8] T. J. McCoy and J. V. Amy, "The state-of-the-art of integrated electric power and propulsion systems and technologies on ships," *Proc. IEEE ESTS*, pp. 340-344, Apr. 2009.

[9] *Electricity Technology Roadmap, 2003*. Palo Alto, CA: Electric Power Research Institute (EPRI), Inc. http://mydocs.epri.com/docs/CorporateDocuments/StrategicVision/Roadmap2003.pdf.

[10] H. Akagi, "Large Static Converters for Industry and Utility Applications," *Proc. of the IEEE*, vol. 89, no. 6, pp. 976-983, Jun. 2001.

[11] H. Akagi, "Active harmonic filters," *Proc. of the IEEE*, vol. 93, no. 12, pp. 2128-2141, Dec. 2005.

[12] A. Yazdani and R. Iravani, "A neutral-point clamped converter system for direct-drive variable-speed wind power unit," *IEEE Trans. on Energy Conv.*, vol. 21, no. 2, pp. 596-607, Jun. 2006.

[13] *Proceedings of Portable Power Developer's Conference (PPDC '05)*, San Jose, CA, Apr. 2005. Corona, CA: Darnell Group Inc., 2005.

[14] R. H. Lasseter and P. Paigi, "Microgrid: a conceptual solution," in *Power Electronics Specialists Conference, 2004. PESC 04. 2004 IEEE 35th Annual*, 2004, pp. 4285-4290 Vol.6.

[15] L. Xuan and S. Bin, "Microgrids - an integration of renewable energy technologies," in *Electricity Distribution, 2008. CICED 2008. China International Conference on*, 2008, pp. 1-7.

[16] J. Bryan, R. Duke and S. Round, "Decentralised control of a nanogrid," presented at *Australasian Universities Power Engineering Conference*, Christchurch, New Zealand, Sep., 2003.

[17] J. Bryan, R. Duke, and S. Round, “Distributed generation – nanogrid transmission and control options,” *International Power Engineering Conference*, vol. 1, pp. 341–346, Nov., 2003.
[18] Z. M. Salameh and A. J. Davis, "Case study of a residential-scale hybrid renewable energy power system in an urban setting," in *Power Engineering Society General Meeting, 2003, IEEE*, 2003, p. 2322 Vol. 4.
[19] I. Cvetkovic, T. Thacker, D. Dong, G. Francis, V. Podosinov, D. Boroyevich, F. Wang, R. Burgos, G. Skutt, and J. Lesko, "Future home uninterruptible renewable energy system with vehicle-to-grid technology," in *Energy Conversion Congress and Exposition, 2009. ECCE 2009. IEEE*, 2009, pp. 2675-2681.
[20] "IEEE Standard for Interconnecting Distributed Resources with Electric Power Systems," *IEEE Std 1547-2003,* pp. 0_1-16, 2003.
[21] T. Sakurai, "Perspectives on power-aware electronics," in *Solid-State Circuits Conference, 2003. Digest of Technical Papers. ISSCC. 2003 IEEE International*, 2003, pp. 26-29 vol.1.
[22] T. Thacker, R. Burgos, F. Wang, and D. Boroyevich, "Single-phase islanding detection based on phase-locked loop stability," in *Energy Conversion Congress and Exposition, 2009. ECCE 2009. IEEE*, 2009, pp. 3371-3377.
[23] D. Dong, T. Thacker, R. Burgos, D. Boroyevich, F. Wang, and B. Giewont, "Control design and experimental verification of a multi-function single-phase bidirectional PWM converter for renewable energy systems," in *Power Electronics and Applications, 2009. EPE '09. 13th European Conference on*, 2009, pp. 1-10.
[24] D. Salomonsson and A. Sannino, "Low-Voltage DC Distribution System for Commercial Power Systems With Sensitive Electronic Loads," *Power Delivery, IEEE Transactions on,* vol. 22, pp. 1620-1627, 2007.
[25] D. Nilsson and A. Sannino, "Efficiency analysis of low- and medium-voltage DC distribution systems," in *Power Engineering Society General Meeting, 2004. IEEE*, 2004, pp. 2315-2321 Vol.2.
[26] P. Karlsson and J. Svensson, "DC bus voltage control for a distributed power system," *Power Electronics, IEEE Transactions on,* vol. 18, pp. 1405-1412, 2003.
[27] H. Kakigano, Y. Miura, T. Ise, and R. Uchida, "DC Micro-grid for Super High Quality Distribution - System Configuration and Control of Distributed Generations and Energy Storage Devices," in *Power Electronics Specialists Conference, 2006. PESC '06. 37th IEEE*, 2006, pp. 1-7.
[28] G. C. Hua, W. A. Tabisz, C. S. Leu, N. Dai, R. Watson, and F. C. Lee, "Development of a DC distributed power system," in *Applied Power Electronics Conference and Exposition, 1994. APEC '94. Conference Proceedings 1994., Ninth Annual*, 1994, pp. 763-769 vol.2.
[29] M. Brenna, G. C. Lazaroiu, and E. Tironi, "High power quality and DG integrated low voltage dc distribution system," in *Power Engineering Society General Meeting, 2006. IEEE*, 2006, p. 6 pp.
[30] W. Schulz, "ETSI standards and guides for efficient powering of telecommunication and datacom," in *Telecommunications Energy Conference, 2007. INTELEC 2007. 29th International*, 2007, pp. 168-173.
[31] T. Aoki, M. Yamasaki, T. Takeda, T. Tanaka, H. Harada, and K. Nakamura, "Guidelines for power-supply systems for datacom equipment in NTT," in *Telecommunications Energy Conference, 2002. INTELEC. 24th Annual International*, 2002, pp. 134-139.
[32] Y. Liu, A. Pratt, P. Kumar, M. Xu, and F. C. Lee, "390V Input VRM for High Efficiency Server Power Architecture," in *Applied Power Electronics Conference, APEC 2007 - Twenty Second Annual IEEE*, 2007, pp. 1619-1624.
[33] D. Yu, Z. Xiaohu, B. Sanzhong, S. Lukic, and A. Huang, "Review of non-isolated bi-directional DC-DC converters for plug-in hybrid electric vehicle charge station application at municipal parking decks," in *Applied Power Electronics Conference and Exposition (APEC), 2010 Twenty-Fifth Annual IEEE*, 2010, pp. 1145-1151.
[34] D. Izquierdo, R. Azcona, F. del Cerro, C. Fernandez, and B. Delicado, "Electrical power distribution system (HV270DC), for application in more electric aircraft," in *Applied Power Electronics Conference and Exposition (APEC), 2010 Twenty-Fifth Annual IEEE*, 2010, pp. 1300-1305.
[35] http://www.us.tdk-lambda.com/
[36] http://www.vicr.com/
[37] J. G. Ciezki and R. W. Ashton, “Selection and stability issues associated with a navy shipboard DC zonal electric distribution system,” *IEEE Trans. on Pow. Del.*, vol.15, no. 2, pp. 665-669, Apr. 2000.
[38] Z. Weidong, S. Pekarek, J. Jatskevich, O. Wasynczuk, D. Delisle, “A model-in-the-loop interface to emulate source dynamics in a zonal DC distribution system,” *IEEE Trans. on Pow. Elec.*, vol. 20, no. 2, pp. 438-445, Mar. 2000.
[39] K. Eriksson, “Operational experience of HVDC Light™,” *Seventh International Conference on AC and DC Transmission*, pp. 205-210, Nov. 2001.
[40] S. D. Wright, A. L. Rogers, J. F. Manwell, and A. Ellis, “Transmission options for offshore wind farms in the United States,” *Proc. AWEA Annual Conference*, Portland, OR, Jun. 2002.
[41] B. R. Andersen, “HVDC transmission - opportunities and challenges,” *8th IEE International Conf. on AC and DC Power Transmission (ACDC 2006)*, pp. 24-29, Mar. 2006.
[42] Y. Xibo, F. Wang, R. Burgos, L. Yongdong, and D. Boroyevich, "Dc-link voltage control of full power converter for wind generator operating in weak grid systems," in *Applied Power Electronics Conference and Exposition, 2008. APEC 2008. Twenty-Third Annual IEEE*, 2008, pp. 761-767.
[43] J. Bryan, R. Duke, and S. Round, "Decentralized generator scheduling in a nanogrid using DC bus signaling," in *Power Engineering Society General Meeting, 2004. IEEE*, 2004, pp. 977-982 Vol.1.
[44] J. Schonberger, R. Duke, and S. D. Round, "DC-Bus Signaling: A Distributed Control Strategy for a Hybrid Renewable Nanogrid," *Industrial Electronics, IEEE Transactions on,* vol. 53, pp. 1453-1460, 2006.
[45] Dong Dong, Ruxi Wang, Dushan Boroyevich, Igor Cvetkovic, “A Two-stage High Power Density Single-phase ac-dc Bi-directional PWM Converter for Renewable Energy System,” presented at the CPES Conference, Blacksburg, April 2010.
[46] http://www.synopsys.com/
[47] R. D. Middlebrook, “Input filter considerations in design and application of switching regulators,” *IEEE IAS ’76*, pp. 366-382, 1976.
[48] X. Feng and F. C. Lee, “On-line measurement of stability margin of dc distributed power system,” *IEEE APEC ’00*, vol. 2, pp. 1190-1196, Mar. 2000.
[49] J. Liu, X. Feng, F. C. Lee, and D. Boroyevich, “Stability margin monitoring for dc distributed power systems via perturbation approaches,” *IEEE Trans. Power Elec.*, vol. 18, no. 6, pp. 1254-1261, Nov. 2003.
[50] A. D. Graham, “Non-characteristic line harmonics of PWM ac-dc converters,” *Proc. Harmonics and Quality of Power.*, vol. 3, pp. 955-960, Oct. 2000.
[51] H. Zhu, R. Burgos, F. Wang, D. Boroyevich, and D. K. Lindner, “Modeling and prediction of dc-bus harmonic resonance for ac-to-ac motor drive systems,” *Conf. AIAA IECEC ’06*, Jun. 2006.
[52] L. Arnedo, R. Burgos, F. Wang, and D. Boroyevich, “Black-box terminal characterization modeling of dc-to-dc converters,” *IEEE APEC ’07*, pp. 457-463, Feb. 2007.
[53] J. A. Oliver, R. Prieto, V. Romero, and J. A. Cobos, "Behavioral modeling of dc-dc converters for large-signal simulation of distributed power systems," in *Applied Power Electronics Conference and Exposition, 2006. APEC '06. Twenty-First Annual IEEE*, 2006, p. 6 pp.
[54] V. Valdivia, A. Barrado, A. Lazaro, C. Fernandez, and P. Zumel, "Black-box modeling of DC-DC converters based on transient response analysis and parametric identification methods," in *Applied Power Electronics Conference and Exposition (APEC), 2010 Twenty-Fifth Annual IEEE*, 2010, pp. 1131-1138.
[55] A. C. Baisden, D. Boroyevich, and F. Wang, "EMI Terminal Modeling," in *Industry Applications Society Annual Meeting, 2008. IAS '08. IEEE*, 2008, pp. 1-8.
[56] Q. Liu, F. Wang, and D. Boroyevich, “Modular-terminal-behavioral (MTB) model for characterizing switching module conducted EMI generation in converter systems,” *IEEE Trans. on Power Electronics*, vol. 21, no. 6, pp. 1804-1814, Nov. 2006.
[57] J. A. Oliver, R. Prieto, J. A. Cobos, O. Garcia, and P. Alou, "Hybrid Wiener-Hammerstein Structure for Grey-Box Modeling of DC-DC Converters," in *Applied Power Electronics Conference and Exposition, 2009. APEC 2009. Twenty-Fourth Annual IEEE*, 2009, pp. 280-285.